NJC

Accepted Manuscript

This is an *Accepted Manuscript*, which has been through the Royal Society of Chemistry peer review process and has been accepted for publication.

Accepted Manuscripts are published online shortly after acceptance, before technical editing, formatting and proof reading. Using this free service, authors can make their results available to the community, in citable form, before we publish the edited article. We will replace this *Accepted Manuscript* with the edited and formatted *Advance Article* as soon as it is available.

You can find more information about *Accepted Manuscripts* in the Information for Authors.

Please note that technical editing may introduce minor changes to the text and/or graphics, which may alter content. The journal's standard Terms & Conditions and the Ethical guidelines still apply. In no event shall the Royal Society of Chemistry be held responsible for any errors or omissions in this *Accepted Manuscript* or any consequences arising from the use of any information it contains.

ROYAL SOCIETY OF CHEMISTRY

www.rsc.org/njc

Fabrication of innovative ZnO nanoflowers showing drastic biological activity

Shaikh M. Mobin,[*1, 2, 3] Vinay Sharma,[1] Akbar Mohammad,[2] Veenu Mishra,[2] Archana Chaudhary[2] and Kshipra Kapoor[2]

[1]Centre for Biosciences and Bio-Medical Engineering, Indian Institute of Technology Indore, Khandwa Road, Indore 452017, India.

[2]School of Basic Sciences, Discipline of Chemistry, Indian Institute of Technology Indore, Khandwa Road, Indore 452017, India.

[3]Material Science and Engineering, Indian Institute of Technology Indore, Khandwa Road, Indore 452017, India.

Email: xray@iiti.ac.in

Abstract

The present work deals with synthesis of ZnO nanoflowers (**ZnO-1** and **ZnO-2)** at room temperature using new structurally characterized single molecular precursors (**1** and **2)**. **1**, **2** and **ZnO-1** were explored for their potential to cause loss of viability to gram-negative bacteria *Escherichia coli.* **1** and **2** were found to be promising antibacterial agents, while the ZnO nanoflowers have shown a relative non-toxic nature. **1**, **2** and **ZnO-1** were further evaluated for DNA binding and cleavage behaviour. **1** and **2** have shown strong binding affinity towards CT-DNA as compare to **ZnO-1**. Additionally, all three of them have shown oxidative cleavage of pBluescript plasmid DNA in the presence of H_2O_2.

Keywords: **Zn(II) complexes; molecular precursors; nanoflowers; antibacterial; DNA binding; DNA cleavage**

1. Introduction

Zn(II) complexes bearing multidentate ligands are actively being pursued owing to their interesting structural aspects[1,2] and widespread applications in catalysis,[3] magnetism[4] as well as in material synthesis.[5,6] Zinc plays a vital role in biological processes[7] such as neuronal activity,[8] treatment of Alzheimer disease,[9] antibacterial,[10] antidiabetic,[11] anti-inflammatory,[12-13] and antitumor effects.[14]

ZnO nanostructures are well known for its wide band gap (3.37eV) among other semiconducting materials. The morphological characteristics of the materials can largely affect their properties. The properties of ZnO are highly dependent on its uniformity in size, shape and aspect ratio which enables the fabrication of devices such as light-emitting diodes (LEDs), piezoelectric, and optoelectronic devices with remarkable optical, electronic, catalytic and sensing properties.[15]

ZnO self-assembled nanostructures with varying morphology have been extensively reported. [16] In general approaches for synthesis of ZnO depends upon hydrothermal, solvothermal, electrochemical and others well-equipped techniques such as physical and chemical vapor deposition, pulsed laser deposition, sputtering, microwave-assisted and template based approach.[17] However, these methods are limited due to their requirement of extreme conditions like high temperature, high cost and sophisticated instrumentation. There are only a few reports available for simple solution based methods using single molecular precursors or complexes.[18,19]

Recently, much attention has been paid to the antimicrobial studies of metal nanoparticles and this field is growing rapidly.[20-22] ZnO nanoparticles have been extensively studied for their growth inhibition properties against various bacterial species,[23] but very few studies have been reported for aforesaid effects with Zinc complexes.[10] Recently, focus on development of antibiotic materials[24-26] has been increased due to evolution of multidrug resistant bacteria.[27] The

binding of metal complexes with DNA is of considerable interest to find out new agents for DNA cleavage.[28] Metal nanoparticles have also been studied for their DNA binding capabilities because of their specificity and reproducibility[29] in numerous applications such as DNA sensors[30] and Biodiagnostics.[31]

Herein, we report room temperature, solution based synthesis of ZnO nanoflowers using new asymmetrical and symmetrical Zn(II) dimers as *single molecular precursors*. Comparative studies on antibacterial effects, DNA binding and DNA cleavage of Zn(II) complexes and ZnO nanoflowers have also been explored.

2. Results and Discussion

2.1 Synthesis and Characterization of Single Molecular Precursors

Asymmetric $[Zn(hmp\text{-}H)_2(H_2O)(\mu\text{-}Cl)Zn(\mu\text{-}Cl)(Cl)_3]$ (**1**) and symmetric $[Zn(hep\text{-}H)(\mu\text{-}Cl)(Cl)]_2$ (**2**) dimers are obtained by the reaction of $ZnCl_2$ with pyridine alcohols, {hmp-H and hep-H (hmp-H=2-(2-hydroxymethyl)pyridine, hep-H=2-(2-hydroxyethyl)pyridine} under mild conditions (Scheme 1). Both the complexes were characterized by FT-IR, elemental analysis, single crystal XRD studies and their thermal stability were investigated by thermogravimetric analysis (Fig. S1).

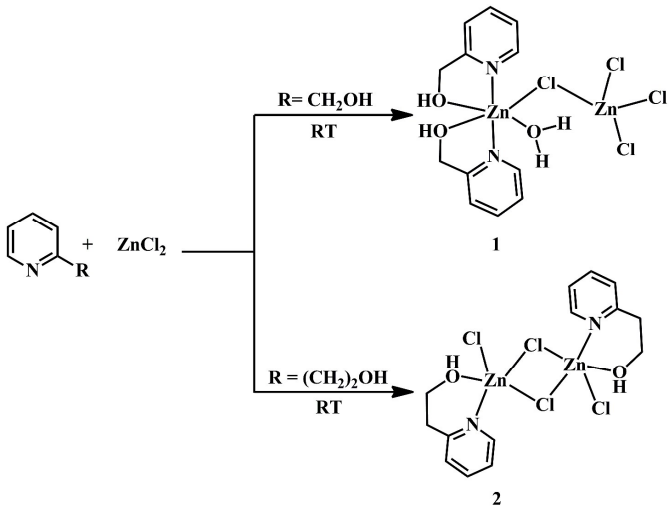

Scheme 1 An outline of the reactions leading to the formations of **1**and **2.**

In asymmetric dimer **1**, two Zn(II) centers are present in hexa- and tetra-coordination environment (Fig. 1) whereas in symmetric dimer **2**, both the Zn(II) ions are penta-coordinated (Fig. 2). In both the complexes hmp-H/hep-H ligands are linked to the Zn centre in bidentatefashion, creating five/six membered rings, respectively.

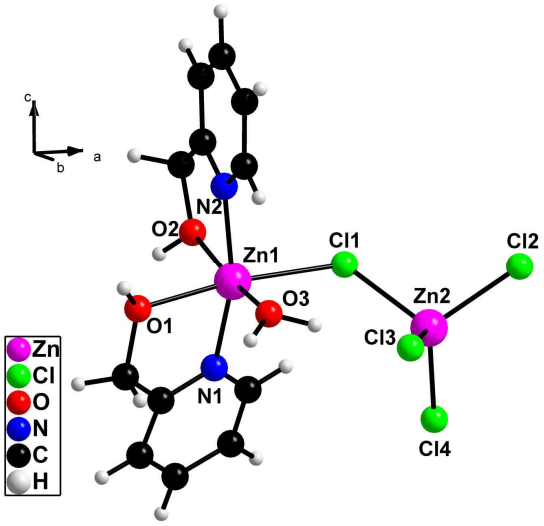

Fig. **1** Crystal structure of compound **1**.

In asymmetric dimer **1** Zn(1) is present in the hexacoordinated environment forming distorted octahedral geometry, out of six coordination sites four are occupied by N, O of the two molecule of hmp-H, one by the μ_2-Cl, and remaining one site is coordinated to the water molecule. Unlike Zn(1), the Zn(2) centre is tetrahedrally coordinated to four Cl-atoms, out of which three Cl atoms are terminal and one is bridging. Zn-Zn separation in **1** is observed to be 4.169Å.

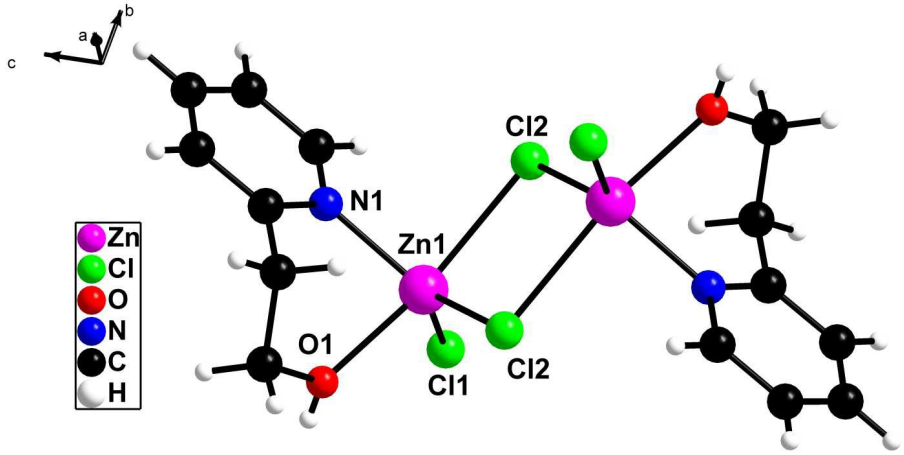

Fig. **2** Crystal structure of compound **2**.

The symmetric dimer **2** shows with distorted square pyramidal geometry around the Zn(II) centres. The basal plane is constituted of N, O atoms of bidentate hep-H, one terminal Cl atom, and apical position is occupied by another bridged Cl atom. In **2,** hep-H ligands are arranged in *trans* fashion creating six membered ring around the metal centre with bite angle 83.13°. Zn-Zn separation in **2** is found to be 3.350Å that is shorter than **1** (Fig. 2, Table S1).

Crystallographic parameters of complexes **1** and **2** are given in Table 1 whereas selected bond lengths and bond angles are summarized in Table S1 and S2.

Table **1.** Crystallographic parameters of complexes **1** and **2**.

Identification code	**1**	**2**
Empirical formula	$C_{12}H_{16}Cl_4N_2O_3Zn_2$	$C_7H_9Cl_2NOZn$
Formula weight	508.81	259.42
Wavelength	0.71073Å	0.71073 Å
Crystal system, space group	Orthorhombic, *Pbca*	Monoclinic, $P2_1/n$
Unit Cell Parameter		
a/Å	9.4731(5)	10.468(7)
b/Å	13.5296(8)	8.1058(6)
c/Å	29.0220(18)	10.993(3)
α/°	90	90
β/°	90	97.69(4)
γ/°	90	90
V/Å^3	3719.7(4)	924.5(7)
Z, d_{calcd} (mg/m^3)	8, 1.817	4, 1.864
μ/ mm^{-1}	3.165	3.182
F(000)	2032	520
θ range	2.98 to 25.00 deg.	3.13 to 25.00 deg
Index ranges	10<=h<=11 -15<=k<=16 -34<=l<=34]	-12<=h<=12 -9<=k<=9 -7<=l<=13
Reflections collected / unique	18005 / 3272 [R(int) = 0.0670]	3961 / 1627 [R(int) = 0.0430]
Max. and min. transmission	0.5996 and 0.4215	0.6468 and 0.5281
Data / restraints / parameters	3272 / 4 / 224	1627 / 0 / 113
GOF, F^2	1.150	0.995
R1, wR2 [I>2σ(I)]	R1 = 0.0467, wR2 = 0.0804	R1 = 0.0372, wR2 = 0.0802
R1, wR2 (all data)	R1 = 0.0622, wR2 = 0.0865	R1 = 0.0451, wR2 = 0.0824
CCDC no.	1050186	1050187

2.2 Synthesis and Characterization of ZnO nanoflowers

ZnO-1 and **ZnO-2** nanostructures with a flower like morphology have been synthesized by an effective simple solution based method using **1** and **2** as precursors. One pot reaction was carried out by dissolving **1** or **2** in distilled water under stirring to form a uniform clear solution at room temperature. To this, an aqueous NaOH solution was added drop wise to form complete precipitation within few minutes. The resulting product was dried at room temperature (Scheme 2) and coded as **ZnO-1** and **ZnO-2**.

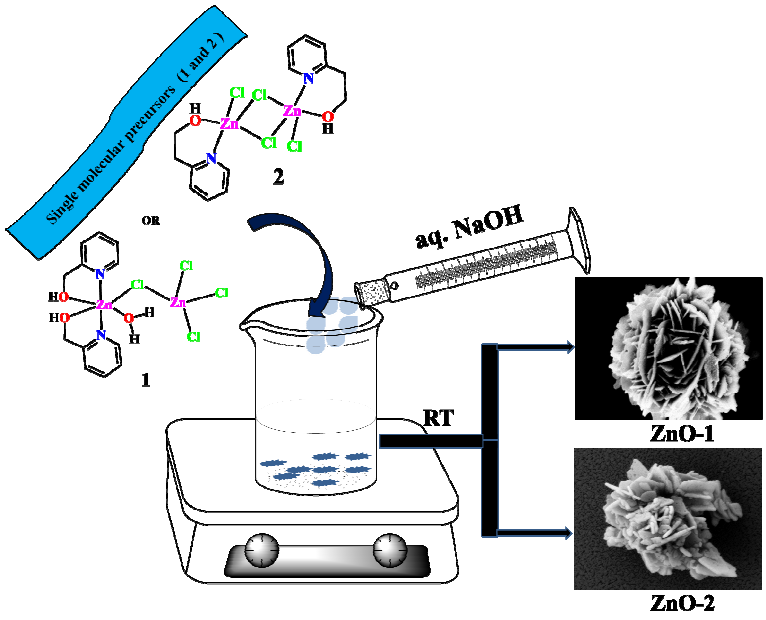

Scheme 2 Schematic diagram for one pot room temperature synthesis of ZnO nanoflowers from designed precursors.

It is interesting to mention here that with both the precursors (**1** and **2)** we obtained the nanoflowers with a slight variation in average crystallite size *i. e.* 30 nm for **ZnO-1** and 46 nm for **ZnO-2**. Further to investigate morphological changes with varying temperature, **ZnO-1** and **ZnO-2** were calcined at 300ºC and 500ºC, producing **ZnO-1a**, **ZnO-1b** and **ZnO-2a**, **ZnO-2b**, respectively.

All the **ZnO** samples were characterized by Powder XRD, UV-Vis spectroscopy, photoluminescence (PL) techniques and surface morphologies were investigated by FESEM images.

The XRD patterns for **ZnO-1, ZnO-1a, ZnO-1b** and **ZnO-2, ZnO-2a, ZnO-2b** reveals that nanostructures prepared at different conditions are crystalline in nature as shown in Fig. 3 and 4. The observed peaks are well indexed as a hexagonal wurtzite structure (JCPDS card No.36-1451). The **ZnO-1** nanostructure which is prepared from **1**, shows completely pure phase, whereas **ZnO-2** nanostructure obtained from **2,** have one additional peak of $Zn(OH)_2$ (JCPDS card No. 38-0385). The average crystallite size of **ZnO-1**, **ZnO-1a** and **ZnO-1b** are 30, 28 and 35nm, respectively and that of **ZnO-2**, **ZnO-2a** and **ZnO-2b** are 46, 42 and 60nm, respectively.

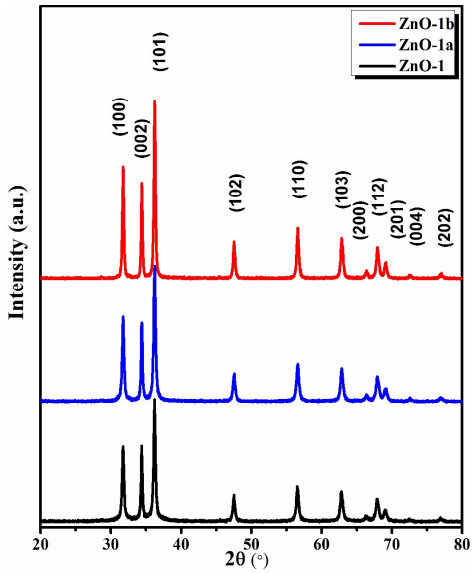

Fig. **3** XRD pattern of ZnO nanoflowers (**ZnO-1**, **ZnO-1a** and **ZnO-1b**) synthesized from **1**.

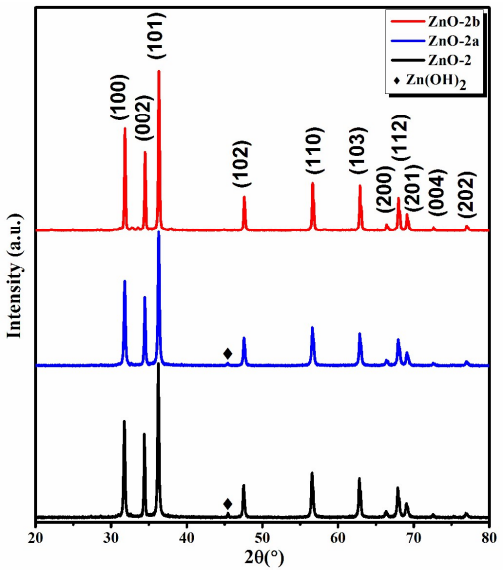

Fig. **4** XRD pattern of ZnO nanoflowers (**ZnO-2**, **ZnO-2a** and **ZnO-2b**) synthesized from **2**.

In terms of crystallinity, no significant difference was observed between room temperature samples and heat treated samples which can be attributed to highly crystalline nature of as synthesized **ZnO-1** and **ZnO-2**.

The crystallite size of **ZnO-1a and ZnO-2a (**heat treated samples at 300°C) was observed slightly less than **ZnO-1** and **ZnO-2**, respectively. The exact reason for reducing average crystallite size at high temperature is not well implicit so far.[32,33]However, at higher temperature at 500°C, energetic crystals get agglomerate with each other and results in increased average crystallite size.[34]

To understand the microstructures of ZnO nanoflowers Field Emission Scanning Electron Microscopy (FE-SEM) imaging was recorded (Fig. 5 and 6). In case of **ZnO-1** the FE-SEM images show uniform ZnO nanostructures with flower like morphology with the size range of approximately ~1.2 μm (Fig. 5). Moreover, nanoflowers have well-organized morphology, consisting of approx. 20 nm leaves which are self-assembled. It should be noted that with varying temperature no considerable change in the surface morphology was observed in samples

ZnO-1a and **ZnO-1b** but varying thickness of leaf was observed as compared to **ZnO-1** (Fig. 5). However, nanoflowers formed by **ZnO-2, ZnO-2a** and **ZnO-2b,** have not shown much effect on surface morphology with temperature, but the nano-leaves within 40-50nm size range were observed (Fig. 6). These leaves are further assembled and led to the formation of nanoflowers.

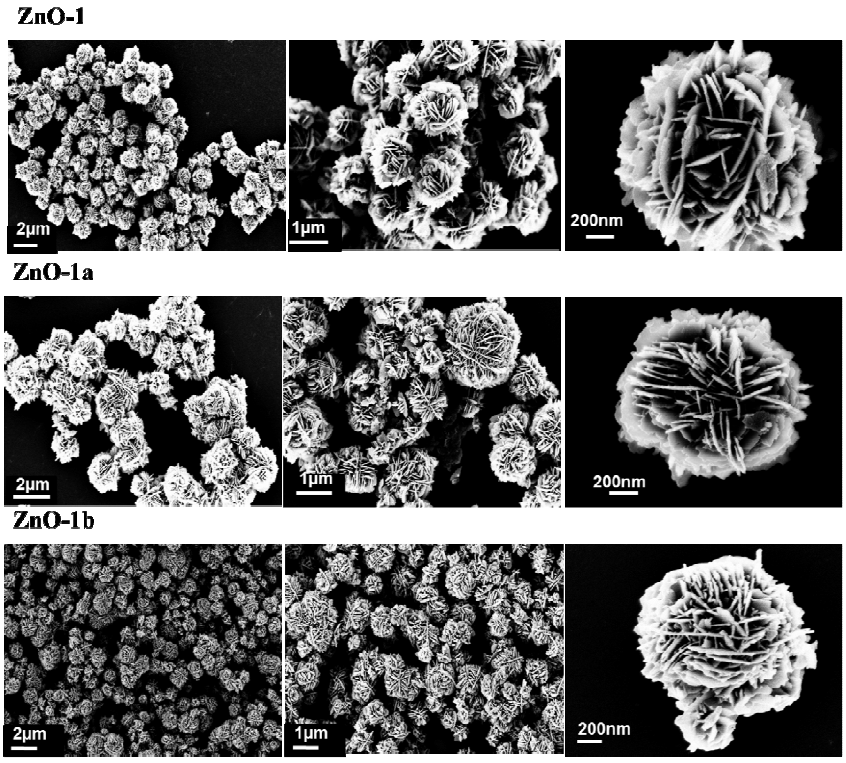

Fig. **5** SEM images of ZnO nanoflowers (**ZnO-1**, **ZnO-1a** and **ZnO-1b**) synthesized from **1**.

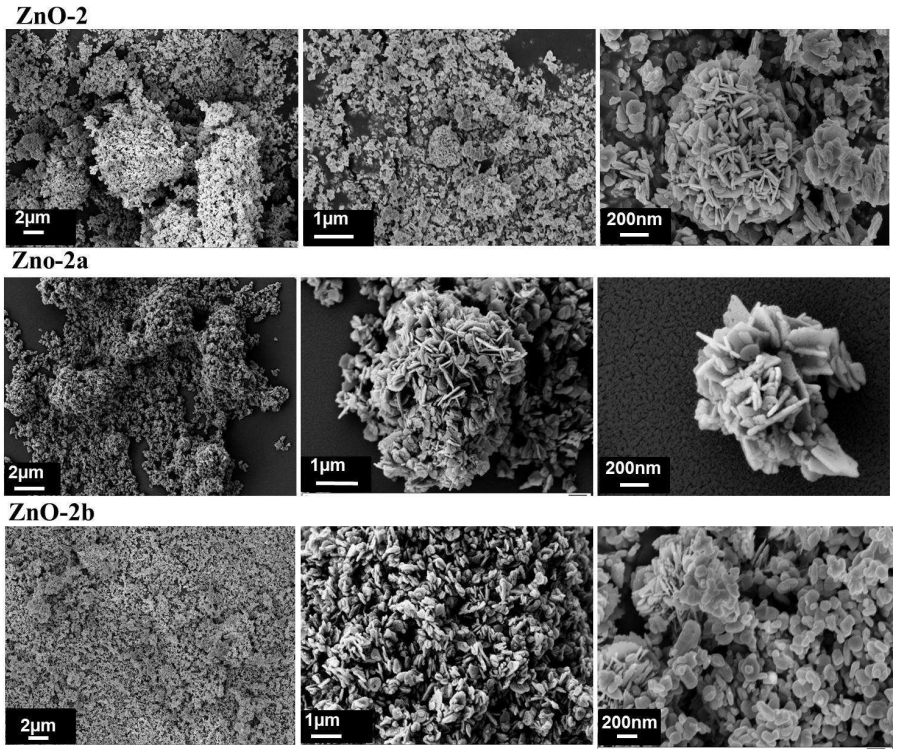

Fig. **6** SEM images of ZnO nanoflowers (**ZnO-2**, **ZnO-2a** and **ZnO-2b**) synthesized from **2**.

As observed in the PXRD data that the average crystallite size is larger in case of **ZnO-2** as compare to **ZnO-1**, due to which self-assembly and uniformity in **ZnO-2** observed to be relatively affected which lead to appearance of smaller size of the **ZnO-2** nanoflowers compared to **ZnO-1**.

The UV-Vis absorption analyses of ZnO samples have been performed, as demonstrated in Fig. 7 and 8. The ZnO nanoflowers **ZnO-1, ZnO-1a** and **ZnO-1b** have characteristics band appeared in the UV region whereas a narrow absorption band was observed for **ZnO-2, ZnO-2a** and **ZnO-2b**. It has been found that the increase in calcination temperature leads to the shift of absorption band from 370 to 385nm.

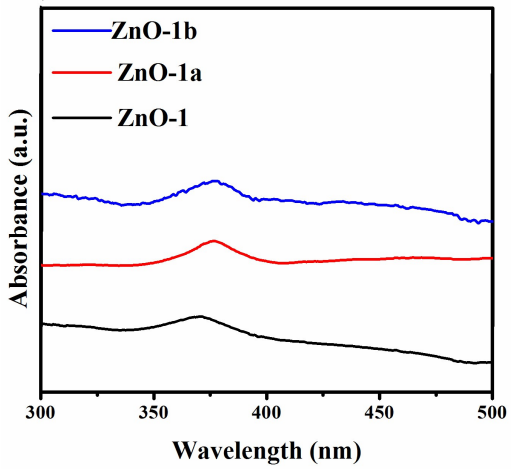

Fig. **7** UV-Vis absorption spectra of ZnO nanoflowers (**ZnO-1**, **ZnO-1a** and **ZnO-1b**) synthesized from **1**.

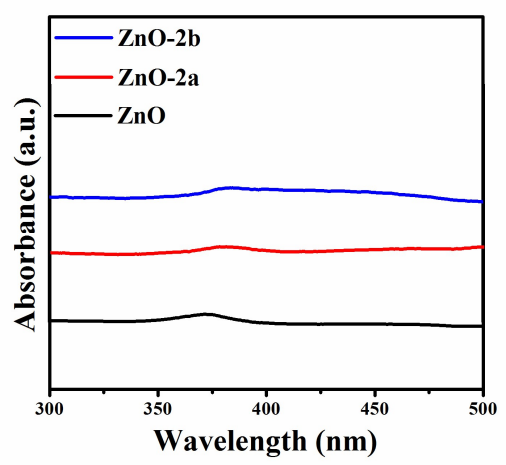

Fig. **8** UV-Vis absorption spectra of ZnO nanoflowers (**ZnO-2**, **ZnO-2a** and **ZnO-2b**) synthesized from **2**.

PL spectra of ZnO nanoflowers are showing two emission bands (Fig. 9 and 10). The first band appeared at 380nm, which corresponds to near band edge emission and the second, an intense and broad green band was observed at 575nm. The first band appeared at 380nm was originated due to the recombination of free excitons in the ZnO near band edge. The broad band

appeared in the visible region is correspond to recombination of photoexcited holes and their morphological defects.[35] The calcined samples show that increase in temperature resulted into decreasing band intensity which may be attributed to decrease in oxygen defects in ZnO nanostructures.[36]

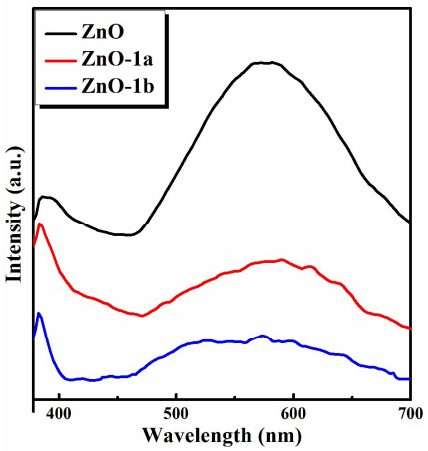

Fig. **9** Room Temperature Photoluminescence spectra of ZnO nanoflowers (**ZnO-1**, **ZnO-1a** and **ZnO-1b**) synthesized from **1**.

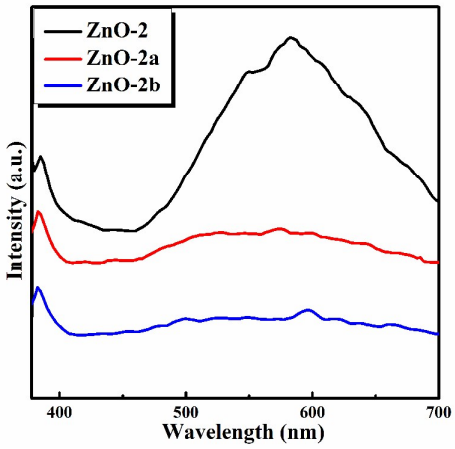

Fig. **10** Room temperature Photoluminescence spectra of ZnO nanoflowers (**ZnO-2**, **ZnO-2a** and **ZnO-2b**) synthesized from **2**.

2.3 Comparative Biological Activities of Molecular Precursors and ZnO nanoflowers

For a better understanding of biological behaviour of molecular precursors as well as ZnO nanoflowers comparative biological studies were performed. **1**, **2** and **ZnO-1** were subjected to biological activities such as antibacterial, DNA binding and DNA cleavage properties. As both the samples (**ZnO-1** and **ZnO-2**) exhibited almost same flower like morphology so ZnO nanoflower with smaller particle-size (*i. e.* **ZnO-1**) was selected for the comparative study.

Gram-negative bacteria, *Escherichia coli* DH5α was used during this study to obtained Minimum Inhibitory Concentration (MIC) and Minimum Bactericidal Concentration (MBC). Fluorescence imaging and FE-SEM microscopy further confirmed the antibacterial behavior. DNA binding was studied with Calf Thymus DNA (CT-DNA). DNA cleavage was performed with plasmid DNA pBluescript.

The Growth inhibition effect of **1, 2** and **ZnO-1** were tested against *E. coli* DH5α. A significant difference in the zone of inhibition formed by **1, 2** and **ZnO-1** was observed at 1000 µg/mL (Fig. S2). The findings of disc diffusion test are summarized in Table **2**.

Table **2.** Size of Zone of Inhibition (in mm) at different concentrations.

Analyte	**Concentration (µg/mL)**								
	300	**400**	**500**	**600**	**1000**	**1400**	**1600**	**1800**	**2000**
Complex 1	No Zone	No Zone	11	11	15	-	-	-	-
Complex 2	No Zone	No Zone	11	11	15	-	-	-	-
ZnO-1	-	-	-	-	No Zone	No Zone	No Zone	No Zone	No Zone

1 and **2** were tested in concentrations range of 300-600µg/mL and **ZnO-1** was tested in concentrations range of 1000-2000 µg/mL, for media turbidity assay. **1** and **2** have shown significant growth inhibition depending upon their concentration while **ZnO-1** was not found much effective even at very high concentration compared to **1** and **2**. MIC was found to be 550µg/mL for both **1** and **2,** which is evident by the reduction in absorbance (Fig. 11), While MBC was found to be 600µg/mL for both **1** and **2**. In case of **ZnO-1**, the growth rate was observed slower than control, but MIC and MBC were not observed upto maximum tested concentration (2000µg/mL).

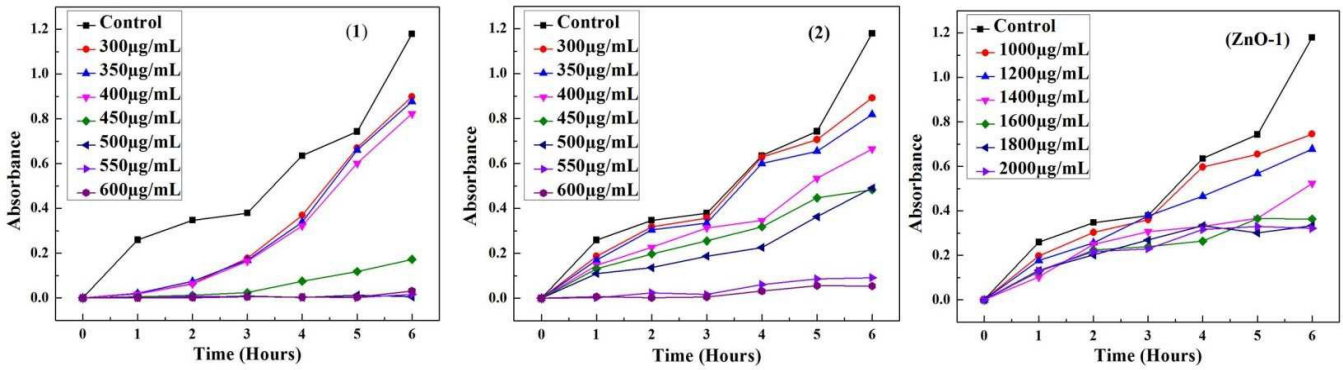

Fig. **11.** Effect of different concentrations of **1**, **2** and **ZnO-1** on growth of *E.coli* DH-5α.

FE-SEM was used to examine the morphological alterations in the bacterial cell wall following the treatment with **1, 2** and **ZnO-1**. Untreated *E.coli* cells appeared to have intact and smooth rod shaped surface morphology, their average length and width being 2µm and 0.5µm respectively. The morphology of cells treated with **1** and **2** has appeared to turn spherical due to stress encountered by cells and average size observed was approx. 500nm. Obvious changes in surface roughness has been observed in cells treated with **ZnO-1**, however many cells retained the rod-shape morphology (Fig. 12).

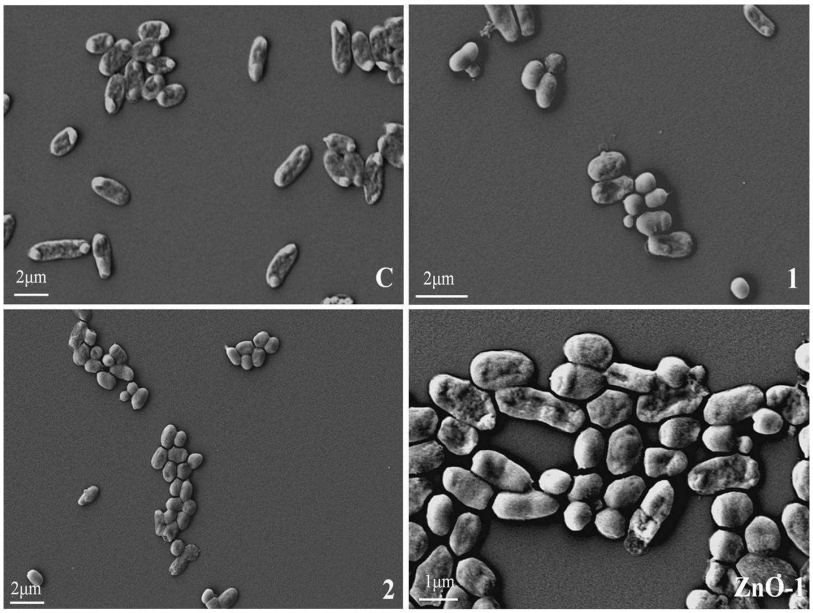

Fig. **12** SEM images of Control, **1**, **2** and **ZnO-1** treated E. *coli* cells.

Fluorescence microscopic analysis revealed that treated cell samples were having significantly high number of dead cells compared to control. Propidium Iodide (PI) binds to DNA by intercalating between the bases. When cell membrane is ruptured, PI stains the cells and gives red fluorescence. Fluorescein Isothiocyanate (FITC) can penetrate the cell membrane and hence it can stain both live and dead cells. Dual stained cells when subjected to fluorescence microscopy yielded following results, Treated cell sample turned into red fluorescence due to high number of dead cells while control cell sample showed green fluorescence indicating viable or live cells with intact cell membrane (Fig. 13).

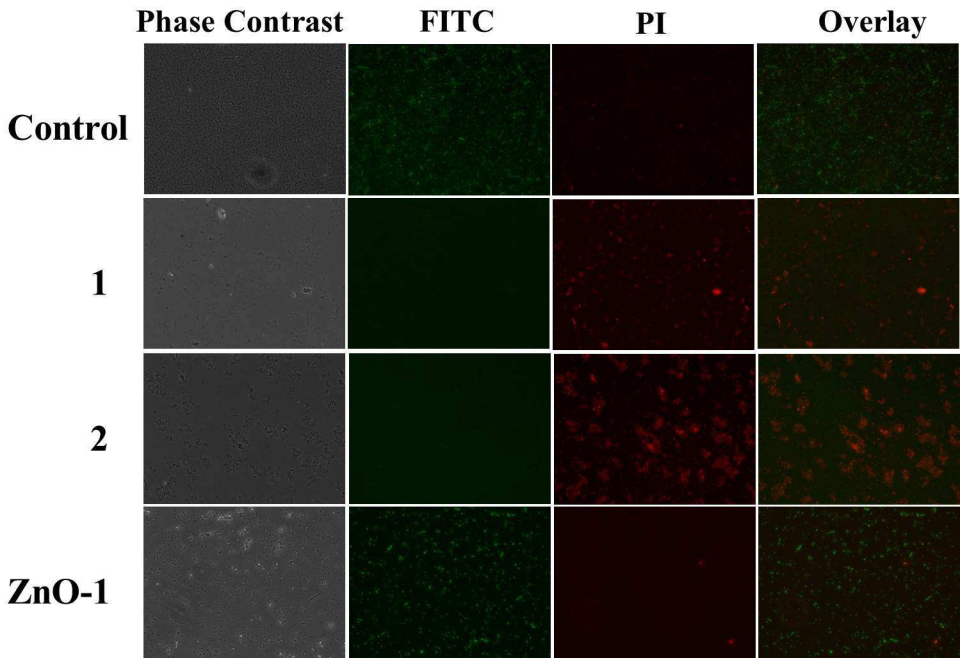

Fig. **13** Fluorescence microscope images of Control, **1**, **2** and **ZnO-1** treated and dual stained *E. coli* cells.

1, 2 and **ZnO-1** were examined for their binding efficiency with calf thymus DNA. In a competitive binding experiment, where ethidium bromide (EtBr) acted as a fluorescent probe while **1, 2** and **ZnO-1** were used as a quencher. Fluorescence quenching results (Fig. S3) were studied by the Stern-Volmer relation,[37] further, the binding constant and number of binding sites are determined by Scatchard equation.[38] The method is described in experimental section. Table **3** represents all relative data.

Data shown in Table **3** clearly indicates that **1** and **2** have almost similar binding tendency towards CT-DNA with a binding constant of the order of 10^2 and number of binding sites almost equal to 1. The interaction of **ZnO-1** is relatively weak with the binding site less than 1 and the binding constant of the order of 10^1. However, the binding constants are relatively on the lower end when compared to different Zn complexes reported so far.[39]

Table **3.** Stern Volmer quenching constant, binding constant and number of binding sites.

Compounds	K_{sv} (M^{-1})	K_a (M^{-1})	*N*
1	3.57 X 10^2	5.57 X 10^2	1.05
2	3.03 X 10^2	7.41 X 10^2	1.12
ZnO-1	2.78 X 10^2	1.38 X 10^1	0.61

To examine the DNA cleavage ability of **1**, **2** and **ZnO-1**, plasmid DNA pBluescript was used. **1**, **2** and **ZnO-1** was incubated with pBluescript DNA for 12 hours in presence and absence of H_2O_2. Agarose gel electrophoresis was performed to observe DNA cleavage (Fig. 14) and it was found that **1**, **2** and **ZnO-1** alone could not damage the DNA (Fig. 14; lane 6-8), while in the presence of H_2O_2, **1**, **2** and **ZnO-1** has the ability to convert the supercoiled form of DNA to a linear form of DNA *i.e.* introducing a double stranded nick in to circular DNA (Fig. 14; lane 3-5). The conversion of super coiled to linear was found more in **1** and **2** in comparison with **ZnO-1**, which is evident by band intensity (Fig. 14; lane 5).

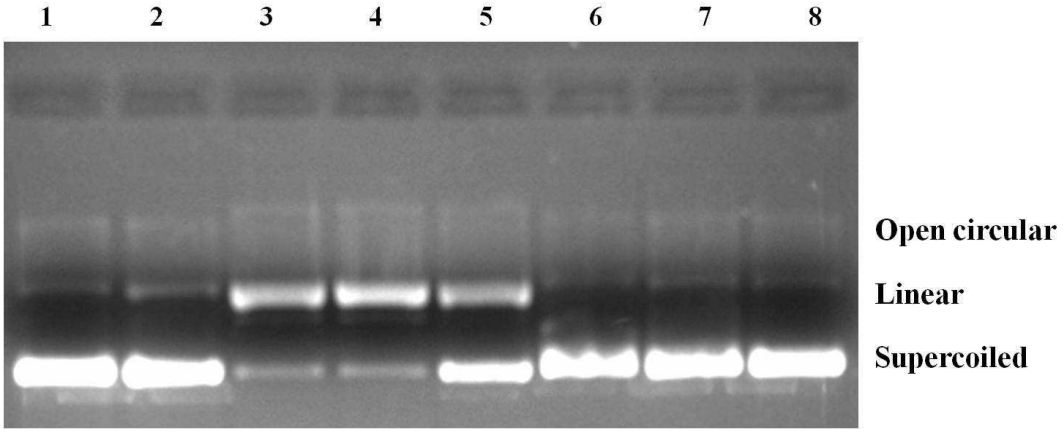

Fig. **14** Gel electrophoresis of DNA cleavage by **1**, **2** and **ZnO-1**. lane 1: plasmid DNA (p); lane 2: p + H_2O_2; lane 3: p + 1 (100μM) + H_2O_2 (60 μM); lane 4: p + 2 (100μM) + H_2O_2 (60 μM); lane 5: p + ZnO-1 (100μM) + H_2O_2 (60 μM); lane 6: p + 1 (100μM); lane 7: p + 2 (100μM); lane 8: p + ZnO-1 (100μM).

Although the exact mode of action for the inhibition in bacterial growth by zinc complexes and ZnO nanostructures is not yet fully understood, many possible mechanisms have been proposed in literature for metal and metal oxide nanoparticles.[40-42] In general, it is believed that both physical and chemical factors play key role in antibacterial actions. Positively charged ions attached to the negatively charged bacterial cell wall. Reactive Oxygen Species (ROS) generated by metal ions ruptures the cell envelope, which in turn leads to leakage and cell death.[40-42] Similarly, in case of **1** and **2**, ROS generated by Zn(II) ions caused cell stress and ruptured the cell wall causing cell death. The antibacterial behaviour of **1** and **2** can also be explained by overtone's concept[43] and chelation theory.[44] The coordination of ligand results into partial sharing of positive charge of zinc ions with the donor group. The decrease in positive charge of zinc ions causes a decrease in polarity of zinc ions which result in increase of lipophilic characters of Zinc ions and support its diffusion into the cell membrane. After entering into the cell, these complexes can block the synthesis of protein and can restrict the growth of bacteria. The DNA binding and DNA cleavage ability of **1** and **2** can also be considered as a major factor for their growth inhibiting effect on bacterial species.

Several studies are available for antibacterial behaviour of ZnO nanostructure and the effect of particle size on antibacterial behaviour has been established by previous studies,[45] it is believed that small particle size facilitate cell permeation, causing leakage and cell death. Previous reports suggest that the antibacterial behaviour of ZnO is due to its surface area and concentration, while the shape and crystalline nature have little effect,[46] It should be noted that the reason for less prominent antibacterial behaviour of **ZnO-1** is its large particle size in flower morphology, due to which it cannot penetrate the bacterial cell wall. Our results are in good agreement with size and surface area dependent antibacterial studies where non porous

micrometer size ZnO have shown little or no antibacterial efficacy.[47] It is worth mentioning here that the synthesized biocompatible ZnO nanoflowers are derived from antibacterial precursors **1** and **2**. Previous reports suggest that some post processing or surface modification such as biomineralisation,[48] carbon coating[49] or functionalization[50] of ZnO nanomaterials lead to reduced toxicity. However, interestingly the as synthesized ZnO nanoflowers (**ZnO-1**) are found relatively less-toxic without any surface modification.

Conclusion

The present study demonstrates a facile one pot room temperature synthesis of ZnO nanoflowers using structurally characterized single molecular precursors. Moreover, the biological activity of **1**, **2** and **ZnO-1** against gram negative bacterial strain *E. coli* DH5α has been evaluated. Molecular precursors **1** and **2** were found to have promising antibacterial properties compared to **ZnO-1**. Additionally, the binding of molecular precursors **1** and **2** with CT-DNA was also found stronger than **ZnO-1**. The study of cleavage of plasmid DNA pBluescript in the presence of H_2O_2 also corroborated the antibacterial and DNA binding results.

Experimental

Materials

The commercially available starting materials, $ZnCl_2$, hmp-H, hep-H, NaOH, Agarose, LB agar, LB broth, CT-DNA, FITC, PI, EtBr and reagent gradesolvents were used without further purification. All chemicals were purchased from Sigma Aldrich and Merck.

Physical measurements

Elemental analyses were carried out with a Flash 2000 elemental analyser. IR spectra [4000–400 cm^{-1}] were recorded with a Bio-Rad FTS 3000MX instrument on KBr pellets. Thermogravimetric analyses were performed on Metler Toledo thermal analysis system. The measurements were done at a heating rate of 10°C/min from 25°C to 900°C under flowing nitrogen environment. Powder X-ray diffraction studies were carried out on Rigaku SmartLab X-ray diffractometer using CuKα radiation (1.54 Å). Uv- visible analysis was conducted using Agilant Cary 60 UV-Visible Spectrophotometer. The room temperature photoluminescence studies were performed on DongwooOptron DM 500i, with excitation wavelength 325 nm. SEM was done using Supra55 Zeiss Field-Emission Scanning Electron Microscope. Fluorescence spectroscopy was performed using FluoroMax spectrofluorometer. Gel image was taken using ImageQuant LAS4000.

Bactericidal studies

For testing the biological activity of **1**, **2** and **ZnO-1**, growth inhibition studies against gram-negative bacteria *Escherichia coli* strain DH5α were carried out in Luria–Bertani (LB) agar and Luria-Bertani broth media. For the disc diffusion test, different concentrations of **1**, **2** (300µg/mL -600µg/mL) and **ZnO-1** (1400µg/mL - 2000µg/mL) were applied to sterile filter paper discs, placing them on inoculated agar plates using sterilized forceps. A comparative plate was also

prepared where the concentration of **1**, **2** and **ZnO-1** was made equal *i.e.*1000µg/mL. The plates were incubated at 37ºC for 16 hours and the zone of inhibition was measured in mm.

For media turbidity assay, sterile 250mL flasks were used, each of them was containing 50mL LB broth media and different concentration of **1**, **2** (300µg/mL - 600µg/mL), and **ZnO-1**(1000µg/mL - 2000µg/mL). Further 500µL of bacterial suspension was added to all flasks as inoculum for maintaining uniform initial bacterial concentration. A positive control (**1**/**2**/**ZnO-1**and nutrient media, without inoculum) and a negative control (Inoculums and nutrient media, without **1**/**2**/**ZnO-1**) were maintained. Experimental flasks were containing nutrient media, inoculums and different concentration of**1**, **2** and **ZnO-1**. The cultures were then placed in incubator shaker at 220rpm and 37°C. Growth kinetics was measured at 600nm based on the absorbance recorded using a spectrophotometer (every hour, upto 6 hours). The absorbance values for experimental flasks were recorded by deducting the corresponding absorbance values for the positive controls.

Bacterial Microscopic Studies

Microscopic analysis of treated and untreated bacterial cells was performed using Fluorescence microscopy and Scanning electron microscopy. Mid log phase *E. coli* cultures were treated with 600µg/mL of **1** and **2**and 1200µg/mL of **ZnO-1** for 6 hrs (Treated bacterial cells). Fluorescence microscopic studies were performed using the method described earlier.[45] Typically, Bacterial cells were stained with propidium iodide (PI) and fluorescein isothiocyanate (FITC) to examine the relative population of live and dead cells. Treated and Control bacterial cells were harvested and the pellets were resuspended in 1mL of 50µg/mL PI in PBS. After incubating at 37ºC for 10 minutes, cells were pellet down and resuspended in 1mL of 2.5µg/mL FITC in PBS. It was further incubated for 10 minutes at 37ºC and then harvested and resuspended in 1mL PBS. 10µL

of prepared suspensions was dropped on a glass slide, mounted with coverslip and used for fluorescence microscopic studies.

SEM was conducted to examine bacterial cell morphology. Treated and untreated bacterial cells were fixed with 2.5% glutaraldehyde in phosphate buffer. Dehydration was carried out by series of ethanol solution (30%, 50%, 70%, 90% and 100%). After dehydration, cells were incubated in 100% ethanol for 1 hr. Finally 10µL from each sample was placed on coverslip and air dried before mounting on SEM stub. Each sample was sputter coated with a thin layer of gold. Digital images were acquired using Supra55 Zeiss Field-Emission Scanning Electron Microscope.

DNA Binding and DNA cleavage studies

Binding of **1**, **2** and **ZnO-1**were studied with Calf Thymus DNA. Tris-HCl buffer (50mM) of pH 7.3 was used during the study. DNA binding for **1**, **2** and **ZnO-1** was measured by EtBr displacement assay whereas fluorescence of EtBr intercalated with CT-DNA was taken as control. The changes in fluorescence intensities were measured at 605 nm of EtBr bound DNA following excitation at 520nm, with a gradual increase in concentration of **1**, **2** and **ZnO-1** (0 to 550µM in steps of 50µM each). EtBr intercalate with DNA bases and emits strong fluorescence in the presence of DNA. When a quencher binds with DNA, it reduces available binding sites for EtBr hence the fluorescence intensity reduces. The increasing concentration of **1, 2** and **ZnO-1** resulted in a gradual reduction in florescence intensity which clearly indicates that **1, 2** and **ZnO-1** are replacing EtBr molecules from their respective binding sites. Fluorescence quenching spectra are shown in **Fig.**S3.Fluorescence quenching results were studied by the Stern-Volmer relation,[37] which is denoted as

$$\frac{F_0}{F} = 1 + K_{sv}[Q] \quad (1)$$

Where F_0 and F are fluorescence intensities in the absence and presence of the quencher (**1, 2** and **ZnO-1**). K_{sv} is the linear Stern–Volmer quenching constant, and [Q] is the concentration of quencher. In the Stern-Volmer plots (inset in **Fig.**S3) of F_0/F versus [Q], the K_{sv}value is given by the slope. The binding constant and number of binding sites are determined by Scatchard equation,[38] which is expressed as

$$\log\left[\frac{F_0 - F}{F}\right] = \log K_a + n\log[Q] \quad (2)$$

Where K_a is binding constant and n is the number of binding sites. The number of binding sites and the binding constant can be determined by the slope and the intercept of the Scatchard plot ($\log(F_0\text{-}F)/F$ vs. log[Q], **Fig.**S4),respectively.

Agarose gel electrophoresis was performed to study DNA cleavage. pBluescript plasmid DNA was incubated at 37º for 12 hrs with 100μM of **1**, **2** and **ZnO-1**in absence and presence of 60μM H_2O_2. After incubation, 6X gel loading dye was added and then loaded on to agarose gel (1%) containing appropriate amount of ethidium bromide. The gel was run for 1 hour at 90V in Tris-acetic acid-EDTA buffer.

X-ray Crystallography

Single crystal X-ray structural studies of **1, 2** were performed on a CCD Agilent technology supernova diffractometer equipped with a low-temperature attachment. Data was collected at 150(2) K using graphite-monochromated Mo Kα radiation (λ_α = 0.71073 Å). The strategy for the Data collection was evaluated by using the CrysAlisPro CCD software. The data were collected

by the standard 'phi-omega scan techniques, and were scaled and reduced using CrysAlisPro RED software. The structures were solved by direct methods using SHELXS-97 and refined by full matrix least squares with SHELXL-97, refining on F^2[51].

The positions of all the atoms were obtained by direct methods andAll non-hydrogen atoms were refined anisotropically. The remaining hydrogen atoms were placed in geometrically constrained positions and refined with isotropic temperature factors, generally 1.2 x U_{eq} of their parent atoms. All the H-bonding interactions, mean plane analyses, and molecular drawings were obtained using the program Diamond (ver 3.1d). The crystal and refinement data are summarized in Table **1** and selected bond distances and bond angles are shown in Table**S1-S2.**

Synthesis of [Zn(hmp-H)$_2$(H$_2$O)(μ-Cl)Zn(μ-Cl)(Cl)$_3$](1)

A solution of hmp-H (0.109 g, 1 mmol) in methanol (5mL) was added to a solution of $ZnCl_2$ (0.136g, 1 mmol) in methanol (35mL) and the resultant solution was stirred for 10h at room temperature. Colourless clear solution was filtered and kept for crystallization. On slow evaporation of the solvent, colourless single crystals of **1** were obtained after 8days. Anal.calcd for $C_{12}H_{16}Cl_4N_2O_3Zn_2$, (Mw =508.81): C 28.57, H 3.20, N 5.55. Found: C 29.24, H 3.50, N 5.74. Mp: 135°C;FT-IR (KBr cm^{-1}) υ= 1699$cm^{-1}_{(C=N)}$, 774$cm^{-1}_{(Zn-O)}$, 568$cm^{-1}_{(Zn-N)}$.

Synthesis of [Zn(hep-H)(μ-Cl)(Cl)]$_2$ (2)

A solution of $ZnCl_2$ (0.136mg, 1 mmol) in methanol (25mL) was added to a solution of hep-H (0.123 mg, 1 mmol) in methanol (5mL) the resultant solution was stirred magnetically for 7h at room temperature. The solution was filtered and kept for crystallization. On slow evaporation of the solvent, colourless single crystals of **2** were obtained after 15 days. Anal.Calcd for $C_7H_9Cl_2NOZn$, (Mw =256.93): C 32.69, H 3.53, N 5.45. Found: C 32.87, H 3.66, N 5.29. Mp: 118°C; FT-IR (KBr cm^{-1}) υ= 1695$cm^{-1}_{(C=N)}$, 770$cm^{-1}_{(Zn-O)}$, 566$cm^{-1}_{(Zn-N)}$.

Synthesis of ZnO-1 and ZnO-2

In general, ZnO-1 and ZnO-2 have been synthesized using simple solution based method. One pot, room temperature reaction was carried out by dissolving 1 mmol of **1** in 20 ml of distilled water under stirring to form a uniform clear solution at room temperature. To this solution, 12 mmol of aqueous NaOH solution (10ml) was added dropwise which led to the complete precipitation within few minutes. The obtained product was washed thrice with distilled water and ethanol by centrifugation at 8000 rpm for 5 minutes each, to remove the unreacted materials and organic volatiles. The resulting product was dried at 50ºC in oven. Finally, **ZnO-1** was calcined at 300ºC (**ZnO-1a**) and 500ºC (**ZnO-1b**).

For the synthesis of **ZnO-2**, the experimental procedure and conditions are same as above. The obtained product **ZnO-2** was calcined at 300ºC (**ZnO-2a**) and 500ºC (**ZnO-2b**).

Acknowledgement

We are grateful to the Sophisticated Instrumentation Centre (SIC), IIT Indore for providing characterization facilities. V.S. thanks UGC for providing research fellowship. A.C. thanks CSIR for providing research fellowship. S.M.M. thanks CSIR, New Delhi for a research grant. Authors wish to thank Dr. Pankaj R. Sagdeo for providing Uv-Vis facility at IIT Indore.

Supplementary materials

Contains other Figures (S1-S4) and Tables (S1 and S2). Crystallographic data for the structural analysis have been deposited with the Cambridge Crystallographic Data Centre, CCDC no's **1050186** and **1050187** for compounds **1** and **2,** respectively.

References

1 H. Furuta, T. Ishizuka and A. Osuka, *J. Am. Chem. Soc.,* 2002, **124**, 5622.

2 D. Samanta and P. Jena, *J. Am. Chem. Soc*., 2012, **134**, 8400.

3 M. A. Fuchs, C. Altesleben, S. C. Staudt, O. Walter, T. A. Zevaco and E. Dinjus, *Catal. Sci. Technol.*, 2014, **4**, 1658.

4 H. L. C. Feltham, F. Klower, S. A. Cameron, D. S. Larsen, Y. Lan, M. Tropiano, S. Faulkner, A. K. Powell and S. Brooker, *Dalton Trans*., 2011, **40**, 11425.

5 C. G. Tian, W. Li, Q. Zhang, K. Pan and H. G. Fu, *Mater. Res. Bull.,* 2011, **46**, 1283.

6 Q. Zhang, C. Tian, A. Wu, T. Tan, L. Sun, L. Wang and H. Fu, *J. Mater. Chem*., 2012, **22**, 11778.

7 G. K. Walkup, S. C. Burdette, S. J. Lippard and R. Y. Tsien, *J. Am. Chem. Soc*., 2000, **122**, 5644.

8 X. Xie and T. G. Smart, *Nature,* 1991, **349**, 521.

9 M. D. Vaira, C. Bazzicalupi, P. Orioli, L. Messori, B. Bruni and P. Zatta, *Inorg. Chem.,* 2004, **43**, 3795.

10 E. Porciatti, M. Milenkovi, E. Gaggelli, G. Valensin, H. Kozlowski, W. Kamysz and D. Valensin, *Inorg. Chem.,* 2010, **49**, 8690.

11 H. Sakurai, Y. Kojima, Y. Yoshikawa, K. Kawabe and H. Yasui, *Coord. Chem. Rev*., 2002, **226**, 187

12 A. Tarushi, X. Totta, C. Raptopoulou, V. Psycharis, G. Psomas and D. P. Kessissoglou, *Dalton Trans*., 2012, **41**, 7082.

13 Q. Zhou, T. W. Hambley, B. J. Kennedy, P. A. Lay, P. Turner, B. Warwick, J. R. Biffin and H. L. Regtop, *Inorg. Chem.,* 2000, **39,** 3742.

14 J. H. Wen, C. Y. Li, Z. R. Geng, X. Y. Ma and Z. L. Wang, *Chem. Commun*., 2011, **47**, 11330.

15 A. B. Djurisic, X. Chen, Y. H. Leung and A. M. C. Ng, *J. Mater. Chem*., 2012, **22** , 6526.

16 S. Cho, S.-H. Jung and K.-H. Lee, *J. Phys. Chem. C*, 2008, **112**, 12769.

17 A. K. Radzimska and T. Jesionowski, *Materials,* 2014, **7**, 2833.

18 J. Xu, Y. Zhu, H. Huang, Z. Xie, D. Chen and G. Shen, *CrystEngComm.,* 2011, **13**, 2629.

19 C. G. Kim, K. Sung, T. M. Chung, D. Y. Jung and Y. Kim, *Chem. Comm.*, 2003, 2068.

20 J. Liu, L. Liu, X. Wu, X. Zhang and T. Li, *New J. Chem.*, 2015, **39**, 5272.

21 W. He, H. K. Kim, W. G. Wamer, D. Melka, J. H. Callahan and J. J. Yin, *J. Am. Chem. Soc.,* 2014, **136**, 750.

22 S. Rtimi, C. Pulgarin, R. Sanjines and J. Kiwi, *RSC Adv.,* 2013, **3**, 16345.

23 A. Sirelkhatim, S. Mahmud, A. Seeni, N. H. M. Kaus, L. C. Ann, S. K. M. Bakhori, H. Hasan and D. Mohamad, *Nano-Micro Lett.,* 2015, **7**, 219.

24 S. Rtimi, O. Baghriche, C. Pulgarin, J-C Lavanchy and J. Kiwi, *Surf. Coat. Technol.,* 2013, **232**, 804.

25 A. Salabat, F. Mirhoseini, M. Mahdieh and H. Saydi, *New J. Chem.*, 2015, **39**, 4109.

26 J. Nesic, S. Rtimi, D. Laub, G. M. Roglic, C. Pulgarin and J. Kiwi, *Colloids Surf., B*, 2014, **123**, 593.

27 B. Spellberg, J. G. Bartlett and D. N. Gilbert, *New Engl. J. Med*., 2013, **368**, 299.

28 W. A. Kalsbeck and H. H. Thorp, *J. Am. Chem. Soc.,* 1993, **115**, 7146.

29 A. Gourishankar, S. Shukla, K. N. Ganesh and M. Sastry, *J. Am. Chem. Soc.,* 2004, **126**, 13186.

30 J. Zhang, S. Song, L. Wang, D. Pan and C. Fan, *Nat. Protoc.,* 2007, **2**, 2888.

31 C. A. Mirkin, *MRS Bulletin,* 2010, **35**, 532.

32 A. Bagabas1, A. Alshammari, M. FA Aboud and H. Kosslick. *Nanoscale Res. Lett.,* 2013, **8**,516.

33 A. Habib, R. Haubner and N. Stelzer. *Mater. Sci. Enger. B*, 2012, **152**, 60.

34 A. Gaber, M. A. Abdel- Rahim, A. Y. Abdel-Latief, M. N. Abdel-Salam. *Int. J. Electrochem. Sci.,* 2014, **9**, 81.

35 J. Yin, F. Gao, C. Wei and Q. Lu, *Sci Rep.,* 2014, 4, 3736

36 X. Zhang, J. Qin, Y. Xue, P. Yu, B. Zhang, L. Wang and R. Liu, *Sci. Rep.,* 2014, 4, 4596.

37 A. Patra, T. K. Sen, A. Ghorai, G. T. Musie, S. K. Mandal, U. Ghosh and M. Bera, *Inorg. Chem*., 2013, **52**, 2880.

38 P. li, M. Niu, M. Hong, S. Cheng and J. Dou, *J. Inorg. Biochem*., 2014, **137**, 101.

39 S. B. Lara, N. P. Chmel, M. T. Zimmerman, L. R. B. Sosa, C. Garino, L. Salassa, A. Rodger, J. L. Brumaghim, I. G. Mora and N. B. Behrens, *Dalton Trans*., 2015, **44**, 3673.

40 T. Xia, M. Kovochich, M. Liong, L. Madler, B. Gilbert, H. Shi, J. I. Yeh, J. I. Zink and A. E. Nel, *ACS Nano.*, 2008, **2**, 2121.

41 E. Hwang, J. Lee, Y. Chae, Y. Kim, B. Kim, B .Sang and M. Gu, *Small*, 2008, **4**, 746.

42 J. A. Lemire, J. J. Harrison and R. J. Turner, *Nature Rev. Microbiol.*, 2013, **11**, 371.

43 A. Kleinzeller, Academic Press, San Diego, 1999, 1.

44 B. G**.** Tweedy, *Phytopathology.,* 1964, **55**, 910.

45 K. R. Raghupathi, R. T. Koodali and A. C. Manna, *Langmuir,* 2011, **27**, 4020.

46 L. Zhang, Y. Jiang, Y. Ding, M. Povey and D. York, *J. Nanopart. Res*., 2007, **9**, 479.

47 T. Gordon, M. Kopel, J. Grinblat, E. Banin and S. Margel, *J. Mater. Chem*., 2012, **22**, 3614.

48 D. Yan, G. Yin, Z. Huang, L. Li, X. Liao, X. Chen, Y. Yao and B. Hao, *Langmuir,* 2011, **27**, 13206.

49 Y. Guo, H. Wang, C. He, L. Qiu and X. Cao, *Langmuir*, 2009, **25**, 4678.

50 A. Hoshino, K. Fujioka, T. Oku, M. Suga, Y. F. Sasaki, T. Ohta, M. Yasuhara, K. Suzuki, K. Yamamoto, *Nano Lett.* 2004, **4,** 2163.

51 G. M. Sheldrick, *ActaCrystallogr., Sect. A.* 2008, *A64,* 112. *Program for Crystal Structure Solution and Refinement;* University of Göttingen: Göettingen, Germany, 1997.

Table of Contents

Fabrication of innovative ZnO nanoflowers showing drastic biological activity

Shaikh M. Mobin,[*1, 2, 3] Vinay Sharma,[1] Akbar Mohammad,[2] Veenu Mishra,[2] Archana Chaudhary[2] and Kshipra Kapoor[2]

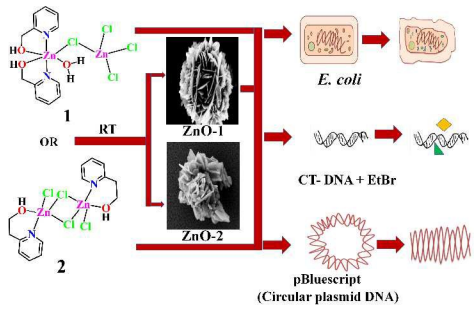

Present article highlights a facile approach towards synthesis of ZnO nanoflowers using designed single molecular precursors (**1** and **2**) at room temperature. Relative biological activities of **1**, **2** and **ZnO** nanoflowers have also been demonstrated.